

NUMERICAL ANALYSIS ON MHD MIXED CONVECTION FLOW OF $\text{Al}_2\text{O}_3/\text{H}_2\text{O}$ (ALUMINUM-WATER) NANOFLUIDS IN A VERTICAL SQUARE DUCT[†]

✉ Bishnu Ram Das[‡], ✉ P.N. Deka[§], ✉ Shiva Rao^{*}

Department of Mathematics, Dibrugarh University, Dibrugarh-786004, Assam, India

[‡]e-mail: bishnuram.das84@gmail.com, [§]e-mail: pndeka@dibru.ac.in

^{*}Corresponding Author e-mail: shivarao374@gmail.com

Received February 9, 2023; revised March 6, 2023; accepted March 9, 2023

In this work, we have considered steady laminar magnetohydrodynamics (MHD) mixed convection flow of an electrically conducting fluid in presence of Al_2O_3 nanoparticle while water is the base fluid in a vertical square duct. The walls of the duct are thermally insulated. In the energy equation, the effect of viscous dissipation and Joule heat are also considered. In this case, the walls of the duct are kept at a constant temperature. By using dimensionless quantities, the governing equations of momentum, induction, and energy are first transformed into dimensionless equations and then the reduced equations are solved using an explicit finite difference approach. The velocity, temperature, and induced magnetic field profiles are plotted graphically to analyze the effect of different flow parameters. It is observed that the nanofluid motion expedites with the increase of the value of the magnetic parameter, Reynolds number, and Prandtl number. The current research may find its application in the numerous industrial as well as cooling sectors. This study observed its importance with the view to increasing the heat transfer efficiency for practical applications relevant to industry and engineering issues. The issues discussed in this study have not been included in the earlier investigation for steady nanofluid flow due to a square duct.

Keywords: *Nanofluids; Explicit finite-difference numerical method (EFDM); MHD flow; Buoyancy force; Mixed convection; square duct; Heat transfer; Magnetic field*

PACS: 44.20.+b, 44.40.+a, 44.30.+v, 47.11.-j, 47.11.Bc

1. INTRODUCTION

Nanofluids which have a wide range of applications in industry are defined as suspensions of solid nanoparticles in some form of organic or inorganic materials in basic fluids which are mainly utilized for heat transfer applications. These nanoparticles improve the heat transfer performance by raising conduction and convection coefficients which enables them to be more effective in various applications. The currently available heat transfer fluids which are used for these purposes including water, ethylene glycol mixture, engine oil, etc., possess poor heat transfer capability. In recent times, the consideration of nanofluids in engineering and industrial applications has drawn a lot of attention from scientists due to their improved thermal properties and advantageous heat transfer characteristics without any pressure drop. As a result of their large thermal conductivity, nanofluids are used in place of base fluids as working fluids nowadays. Mixed convection flow is the combination of forced and natural convection flows. Further, mixed convection flow in a channel or duct is encountered in the Dual-Coolant Lead-Lithium (DDCL) flow for fusion power as a tritium breeder and many industrial applications and engineering devices such as a cooling systems for electronic components and reactors. Choi and Eastman [1] introduced the concept of nanofluids and presented impressive results with many possibilities for usage. Nanofluids are new classes of nano-technology-based materials concerning nanoparticles (1nm to 100 nm) dispersed in base fluids. These heat transfer fluids have promoted great interest among researchers in the last few years, mainly due to their potential applications. The nanofluids have higher thermal conductivities in comparison to the base fluids, which could result in higher heat transfer rates.

Convection process in a square duct is relevant to certain heat transfer engineering applications acting as electronic equipment, food drying, heat exchangers, cooling, and nuclear reactors. Experimentally and numerically in recent years, many researchers have studied natural convection and mixed convection in a square duct under a wide range. The mixed convection of $\text{Al}_2\text{O}_3/\text{water}$ nano fluid interior of a square duct accommodates boiling quadrilaterals obstacles on its bottom wall considered by Doustdar and Yekani [2]. Mixed convection flows in a square duct partially heated from below using nanofluid were studied by Mansour et al. [3]. The results of a numerical study on the mixed convection in a square duct filled with a $\text{Al}_2\text{O}_3/\text{water}$ nanofluid was investigated by Ghasemi and Aminossadati [4]. They concluded that the heat transfer rate can be reduced by adding a considerable amount of nanoparticles into the distilled water cases of upward and downward sliding walls. Abu-Nada and Oztop [5] investigated the effect in natural convection processes with nanofluid which are enclosed in containers. Hemmat Esfe et al. [6] studied the heat transfer and Mixed-convection fluid flow of an $\text{Al}_2\text{O}_3/\text{water}$ nanofluid with effective thermal conductivity and viscosity is dependent on temperature and nanoparticle concentration core of a square duct. Their results stipulated that adding Al_2O_3 nanoparticle produces an extraordinary enhancement of heat transfer concerning that of the unmixed fluid. The effect of the Prandtl number and Reynolds number for laminar mixed convection in a top wall moving, the bottom heated square duct was discussed by Moallemi and Jang [7]. They investigated that when Reynolds number and Grashof numbers were kept constant, increment of Prandtl number enhanced the heat transfer rate. The mixed convection in a square duct having a side wall

[†] Cite as: B.R. Das, P.N. Deka, and Shiva Rao, East Eur. J. Phys. 2, 51 (2023), <https://doi.org/10.26565/2312-4334-2023-2-02>

© B.R. Das, P.N. Deka, S. Rao, 2023

moving and a local heat source at the bottom wall was investigated by Yang and Aydin [8]. Analyzed mixed convection for a square duct with both side walls moving by Dagtekin and Oztop [9]. They conducted the study for three different configurations based on the direction of moving walls. Wong and De Leon [10] carried out a review paper detailing the current and future applications of nanofluids. Li et al. [11] investigated the forced convective heat transfer of nanofluids in solar collectors during the day and night, with distilled water and nanoparticles of Al_2O_3 , ZnO , and MgO . The nanofluid achieved a 3°C temperature difference during the daytime peak solar radiation compared with the base fluids. With a concentration of 0.2% ZnO , a temperature difference of 2.55°C for daytime and 1°C for nighttime was reached, and this was determined to be the most attractive option for solar energy utilization. Tooraj et al. [12] witnessed a 28% performance improvement in a flat plate collector when it was operated with $\text{Al}_2\text{O}_3/\text{water}$ nanofluids. Otanicar [13] studied the economic and environmental influences of using nanofluids to enhance solar collector efficiency with conventional solar collectors. The thermophysical properties of the nanofluid are calculated density by Pak and Cho [14], and thermal conductivity by Yu and Choi [15]. The specific heat of the nanofluid is calculated by Xuan and Roetzel [16]. The 3D flow of MHD nanofluid with varied nanoparticles including Fe_3O_4 , Cu , Al_2O_3 and TiO_2 and water as the base fluid past an exponentially stretched surface was discussed by Jusoh et al. [17]. Hung et al. [18] indicated that $\text{Al}_2\text{O}_3/\text{Water}$ nanofluids require less pumping power, followed by CuO/Water nanofluid and $\text{TiO}_2/\text{Water}$ nanofluid for 1% nanoparticle volume concentration. The computed numerical results are presented graphically for velocity, temperature, and induced magnetic field for different flow parameters.

Sheikhpour et al. [19] examined the role of nanofluids in drug delivery and biomedical technology. Majumder and Das [20] presented a short review of organic nanofluids preparation, surfactants, and applications. Dehaj et al. [21] observed the efficiency of the parabolic solar collector using $\text{NiFe}_2\text{O}_4/\text{water}$ nanofluid and U-tube. Sivaraj and Banerjee [22] studied the transport properties of non-Newtonian nanofluids and applications, and Thumma et al. [23] examined that generalized differential quadrature analysis of unsteady three-dimensional MHD radiating dissipative Casson fluid conveying tiny particles. Lahmar et al. [24] analyzed heat transfer by squeezing unsteady nanofluid flow under the effects of an inclined magnetic field and variable thermal conductivity. Rosca and Pop [25] studied hybrid nanofluid flows determined by a permeable power-Law stretching/shrinking sheet modulated by orthogonal surface shear. Selimefendigil and Oztop [26] examined thermal management and modeling of forced convection and entropy generation in a vented cavity by simultaneous use of a curved porous layer and magnetic field. Jamshed studied [27] the numerical investigation of MHD impact on Maxwell nanofluid. Jamshed et al. [28] observed the computational framework of Cattaneo-Chritov heat flux effects on Engine Oil-based Williamson hybrid nanofluids. Jamshed studied [29] that thermal augmentation in solar aircraft using tangent hyperbolic hybrid nanofluid: a solar energy application. Rao and Deka [30] took the Buongiorno model to analyze the heat and mass transfer phenomena of Williamson nanofluid past a moving cylinder. Recently, Rao and Deka [31] made a numerical investigation on the unsteady MHD Casson nanofluid flow caused due to a porous stretching sheet and found that thermal radiation played a very important role in the heat transfer character of the fluid.

Yusuf et al. [32] investigated entropy generation on flow and heat transfer of a reactive MHD Sisko fluid through inclined walls with a porous medium. Hamzah et al. [33] studied MHD mixed convection and entropy generation of CNT-water nanofluid in a wavy lid-driven porous enclosure at different boundary conditions. Khan et al [34] analyzed the analytical assessment of $(\text{Al}_2\text{O}_3\text{-Ag}/\text{H}_2\text{O})$ hybrid nanofluid influenced by induced magnetic field for second law analysis with mixed convection, viscous dissipation, and heat generation. Ahmed and Pop [35] investigated mixed convection boundary layer flow from a vertical flat plate embedded in a porous medium filled with nano-fluids. Malvandi and Ganji [36] studied the mixed convection of alumina-water nanofluid inside a concentric annulus considering nanoparticle migration. Tayebi et al. [37] studied the Magnetohydrodynamic natural convection heat transfer of a hybrid nanofluid in a square enclosure in the presence of a wavy circular conductive cylinder. Shah et al. [38] examined radiative MHD Casson nanofluid flow with activation energy and chemical reaction over past nonlinearly stretching surfaces through entropy generation. Rajesh et al. [39] observed that hydromagnetic effects on hybrid nanofluid $\text{Cu} - \text{Al}_2\text{O}_3/\text{water}$ flow with convective heat transfer due to a stretching sheet. Molli and Naikoti [40] studied the MHD natural convective flow of Cu/water nanofluid over a past infinite vertical plate with the presence of time-dependent boundary conditions. Khashi [41] concludes that flow and heat transfer of hybrid nanofluid over a permeable shrinking cylinder with Joule heating. Alighamdi [42] studied the boundary layer stagnation point flow of the Casson hybrid nanofluid over an unsteady stretching surface. Shahzad et al. [43] observed computational investigation of magneto-cross fluid flow with multiple slips along wedge and chemically reactive species, and Ibrar et al. [44] discovered the interaction of single and multi-walls carbon nanotubes in magnetized-nano Casson fluid over radiated horizontal needle. Lund et al. [45] analyzed the effects of Stefan blowing and slip conditions on unsteady MHD Casson nanofluid flow over an unsteady shrinking sheet. Recently, Rao and Deka [46] studied the numerical investigation of transport phenomena in a nanofluid under the transverse magnetic field over a stretching plate associated with solar radiation. Rao and Deka [47] investigated numerical solution using EFD for unsteady MHD radiative Casson nanofluid flow over a porous stretching sheet with stability analysis.

The present paper aims to investigate the laminar steady MHD mixed convection flow of an electrically conducting fluid in a vertical square duct in the presence of a strong transverse magnetic field using a finite difference scheme. The walls of the duct are assumed as thermally insulating and walls have a constant temperature. The local balance equations

of momentum, magnetic induction, and energy are solved numerically by the finite difference method using the Hartmann number (Ha), Grashof number (G_r), Reynolds number (R_e), Prandtl number (P_r), and magnetic Reynolds number (R_m) as the parameters. The computed numerical results are presented graphically for velocity, temperature, and induced magnetic field for flow parameters.

- To consider a suitable mathematical model involving governing equations and boundary conditions for the nanofluid MHD flow across the square duct.
- Nondimensionalization of the governing equations and performance of the explicit finite difference method.
- Plotting graph for the velocity, temperature, and induced magnetic field distribution for different physical parameters.
- We will compare the obtained results with previous work to validate the efficiency of the numerical approach.

Table 1. Thermo-physical numerical values of water (H_2O) and aluminum (Al_2O_3)

	Density (ρ)	Specific heat capacity (C_p)	Thermal conductivity (k)	Electrical conductivity (σ)
Al_2O_3	3970	765	40	35×10^6
H_2O	997.1	4179	0.613	0.05

2. MATHEMATICAL FORMULATION AND SOLUTIONS

Description of geometry

The steady laminar flow of a Newtonian fluid in a vertical square duct with a uniform horizontal magnetic field of constant intensity B_0 applied transverse to the duct walls is considered.

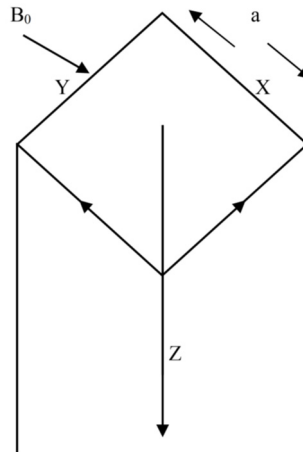


Figure 1. Physical model and the coordinate system

Let a be the length of the cross-section of the duct. It is assumed that the fluid occupies an area between $x = 0$, $x = a$; and $y = 0$, $y = a$. The flow is to be consumed by a constant pressure slope $\frac{\partial p}{\partial z}$ and is constrained to proceed in the z -direction. T_0 is a uniform temperature at the walls of the duct is simulate. By the axiom of fully developed flow, the velocity and temperature fields are side by side, and the only non-vanishing fundamental of velocity and temperature $V_z(x, y)$ and $T(x, y)$ are side by side to the duct axis and independent of the perpendicular coordinate. The uniform horizontal applied magnetic field of force B_0 acts along the y -direction and it induces a magnetic field $B_z(x, y)$ in the flow direction. In this study, an electrically conducting fluid flows along the axis of the duct under the influence of an externally imposed pressure gradient and the Lorentz forces caused by the interaction of the flow with the uniform magnetic field, directed along y . Buoyancy forces, caused by density changes that result from temperature variation, can easily be included thus giving rise to mixed MHD convection.

The following assumptions are made in this study:

- The flow is steady, fully developed and fluid is Newtonian.
- The duct is considered to be infinite so that all the fluid properties except the pressure gradient are independent of the variable z .

The velocity \vec{V} , magnetic field \vec{B} and temperature T shall be the ensuing form

$$\vec{V} = \{0, 0, V_z(x, y)\}, \vec{B} = \{0, B_0, B_z(x, y)\}, T = T(x, y)$$

3. GOVERNING EQUATIONS

The equation of continuity is

$$(\nabla \cdot \vec{V}) = 0. \quad (1)$$

The Momentum equation is

$$\rho_{nf} \left[\frac{\partial \vec{V}}{\partial t} + (\vec{V} \cdot \nabla) \vec{V} \right] = -\nabla p + \mu_{nf} \nabla^2 \vec{V} + (\vec{J} \times \vec{B}) + g(\rho\beta)_{nf}(T - T_o). \quad (2)$$

Maxwell's equation is

$$\nabla \cdot \vec{B} = 0, \quad (3)$$

$$\nabla \times \vec{B} = (\mu_e)_{nf} \vec{J}. \quad (4)$$

Ohm's law:

$$\vec{J} = \sigma_{nf} (\vec{E} + \vec{V} \times \vec{B}). \quad (5)$$

The magnetic induction equation is given by

$$\frac{\partial \vec{B}}{\partial t} = \nabla \times (\vec{V} \times \vec{B}) + \lambda_{nf} \nabla^2 \vec{B}. \quad (6)$$

Now using equations (1) and (3) in (6) we have

$$\frac{\partial \vec{B}}{\partial t} + (\vec{V} \cdot \nabla) \vec{B} = (\vec{B} \cdot \nabla) \vec{V} + \lambda_{nf} \nabla^2 \vec{B}. \quad (7)$$

The energy equation or temperature equation:

$$(\rho C_p)_{nf} \left[\frac{\partial T}{\partial t} + (\vec{V} \cdot \nabla) T \right] = k_{nf} \nabla^2 T + \mu_{nf} \phi + \frac{J^2}{\sigma_{nf}}, \quad (8)$$

where

$$\nu_{nf} = \frac{\mu_{nf}}{\rho_{nf}}, \quad (9)$$

$$\lambda_{nf} = \frac{1}{\sigma_{nf} (\mu_e)_{nf}}. \quad (10)$$

Brinkman's [48] model for the dynamic viscosity of nanofluid is

$$\mu_{nf} = \frac{\mu_f}{(1-\phi)^{2.5}}. \quad (11)$$

Following Khan [49], the effective density of nanofluid is considered as

$$\rho_{nf} = \left[1 - \phi + \phi \frac{\rho_s}{\rho_f} \right] \rho_f. \quad (12)$$

The effective magnetic permeability of nanofluid is given by

$$(\mu_e)_{nf} = \left[1 - \phi + \phi \frac{(\mu_e)_s}{(\mu_e)_f} \right] (\mu_e)_f. \quad (13)$$

Maxwell [50] gives the electrical conductivity of nanofluid

$$\sigma_{nf} = \left[1 + \frac{3(\sigma-1)\phi}{(\sigma+2)-(\sigma-1)\phi} \right] \sigma_f. \quad (14)$$

The heat capacitance of the nanofluid is given [51] by Khanafer

$$(\rho C_p)_{nf} = \left[1 - \phi + \phi \frac{(\rho C_p)_s}{(\rho C_p)_f} \right] (\rho C_p)_f. \quad (15)$$

The thermal expansion coefficient of nanofluid is

$$(\rho\beta)_{nf} = (1 - \phi)(\rho\beta)_f + \phi(\rho\beta)_s. \quad (16)$$

Maxwell-Garnet determined the thermal conductivity of nanofluid

$$k_{nf} = \left[\frac{k_s + 2k_f - 2\phi(k_f - k_s)}{k_s + 2k_f + \phi(k_f - k_s)} \right] k_f, \quad (17)$$

where k_s and k_f are solid and fluid thermal conductivity respectively.

Using velocity, temperature, and current density distribution stated above for steady case, equations (2), (7), and (8) give

$$\frac{1}{(1-\phi)^{2.5}} \mu_f \left[\frac{\partial^2 V}{\partial x^2} + \frac{\partial^2 V}{\partial y^2} \right] + \frac{B_o}{\left[1-\phi + \phi \frac{(\mu_e)_s}{(\mu_e)_f} \right] (\mu_e)_f} \frac{\partial B}{\partial y} + \left[1 - \phi + \phi \frac{\rho_s}{\rho_f} \right] \rho_f g \beta_f (T - T_o) - \frac{\partial p}{\partial z} = 0, \tag{18}$$

$$\frac{1}{\left[1-\phi + \phi \frac{(\mu_e)_s}{(\mu_e)_f} \right] (\mu_e)_f \left[1 + \frac{3(\sigma-1)\phi}{(\sigma+2)-(\sigma-1)\phi} \right] \sigma_f} \left[\frac{\partial^2 B}{\partial x^2} + \frac{\partial^2 B}{\partial y^2} \right] + B_o \frac{\partial V}{\partial y} = 0, \tag{19}$$

$$\left[\frac{k_s + 2k_f - 2\phi(k_f - k_s)}{k_s + 2k_f + \phi(k_f - k_s)} \right] k_f \left[\frac{\partial^2 T}{\partial x^2} + \frac{\partial^2 T}{\partial y^2} \right] + \frac{1}{(1-\phi)^{2.5}} \mu_f \left[\left(\frac{\partial V}{\partial x} \right)^2 + \left(\frac{\partial V}{\partial y} \right)^2 \right] + \frac{1}{((\mu_e)_f)^2 \left[1-\phi + \phi \frac{(\mu_e)_s}{(\mu_e)_f} \right]^2 \left[1 + \frac{3(\sigma-1)\phi}{(\sigma+2)-(\sigma-1)\phi} \right] \sigma_f} \left[\left(\frac{\partial B}{\partial x} \right)^2 + \left(\frac{\partial B}{\partial y} \right)^2 \right] = 0. \tag{20}$$

The corresponding boundary conditions are:

$$\begin{aligned} V_z &= 0, & B_z &= 0, & T &= T_o, & \text{at } y &= 0, \\ V_z &= 0, & B_z &= 0, & T &= T_o & \text{at } y &= a, \text{ for } 0 \leq x \leq b, \\ V_z &= 0, & B_z &= 0, & T &= T_o, & \text{at } x &= 0, \\ V_z &= 0, & B_z &= 0, & T &= T_o, & \text{at } x &= a, \text{ for } 0 \leq y \leq b. \end{aligned} \tag{21}$$

The above equations (18), (19), and (20) can be transformed into dimensionless parameters that are defined

$$\bar{x} = \frac{x}{a}, \bar{y} = \frac{y}{a}, \bar{V} = \frac{V}{V_o}, \bar{B} = \frac{B}{B_o}, \bar{T} = \frac{T - T_o}{\Delta T}. \tag{22}$$

Where $B_o = -a^2 (\mu_e)_{nf} \sqrt{\frac{\sigma_{nf}}{\rho_{nf} \nu_{nf}}} \frac{\partial p}{\partial z}$, $V_o = -\frac{a^2}{\rho_{nf} \nu_{nf}} \frac{\partial p}{\partial z}$, $\Delta T = \frac{V_o^2}{c_p}$,

Using dimensionless quantities (22) in equations (18), (19), and (20) and release bullet, become

$$\frac{\partial^2 V}{\partial x^2} + \frac{\partial^2 V}{\partial y^2} + \frac{B_o^2 a^2 \left[1 + \frac{3(\sigma-1)\phi}{(\sigma+2)-(\sigma-1)\phi} \right] \sigma_f (1-\phi)^5}{V_o a \left[1-\phi + \phi \frac{(\mu_e)_s}{(\mu_e)_f} \right] (\mu_e)_f \left[1 + \frac{3(\sigma-1)\phi}{(\sigma+2)-(\sigma-1)\phi} \right] \sigma_f} \frac{\partial B}{\partial y} + \frac{g \beta_f a^3 (T - T_o)}{V_o^2} \cdot \frac{V_f}{V_o a} + 1 = 0, \tag{23}$$

$$\frac{\partial^2 B}{\partial x^2} + \frac{\partial^2 B}{\partial y^2} + V_o a \left[1 - \phi + \phi \frac{(\mu_e)_s}{(\mu_e)_f} \right] (\mu_e)_f \left[1 + \frac{3(\sigma-1)\phi}{(\sigma+2)-(\sigma-1)\phi} \right] \sigma_f \frac{\partial V}{\partial y} = 0, \tag{24}$$

$$\begin{aligned} \frac{\partial^2 T}{\partial x^2} + \frac{\partial^2 T}{\partial y^2} + \frac{\mu_f c_p}{(1-\phi)^{2.5} k_f \left[\frac{k_s + 2k_f - 2\phi(k_f - k_s)}{k_s + 2k_f + \phi(k_f - k_s)} \right]} \cdot \frac{V_o^2}{c_p \Delta T} \left[\left(\frac{\partial V}{\partial x} \right)^2 + \left(\frac{\partial V}{\partial y} \right)^2 \right] + \\ \frac{B_o^2 a^2 \left[1 + \frac{3(\sigma-1)\phi}{(\sigma+2)-(\sigma-1)\phi} \right] \sigma_f}{V_o^2 a^2 \left[1-\phi + \phi \frac{(\mu_e)_s}{(\mu_e)_f} \right]^2 \left[1 + \frac{3(\sigma-1)\phi}{(\sigma+2)-(\sigma-1)\phi} \right] \sigma_f^2 (\mu_e)_f^2 \left[\frac{k_s + 2k_f - 2\phi(k_f - k_s)}{k_s + 2k_f + \phi(k_f - k_s)} \right]} \cdot \frac{\mu_f c_p}{k_f} \cdot \frac{V_o^2}{c_p \Delta T} \left[\left(\frac{\partial B}{\partial x} \right)^2 + \left(\frac{\partial B}{\partial y} \right)^2 \right] = 0. \end{aligned} \tag{25}$$

Let

$$E_1 = \frac{1}{(1-\phi)^{2.5}}, E_2 = \left[1 - \phi + \phi \frac{\rho_s}{\rho_f} \right], E_3 = \left[1 - \phi + \phi \frac{(\mu_e)_s}{(\mu_e)_f} \right], E_4 = \left[1 + \frac{3(\sigma-1)\phi}{(\sigma+2)-(\sigma-1)\phi} \right], E_5 = \left[1 - \phi + \phi \frac{(\rho c_p)_s}{(\rho c_p)_f} \right], E_6 = \left[\frac{k_s + 2k_f - 2\phi(k_f - k_s)}{k_s + 2k_f + \phi(k_f - k_s)} \right].$$

Therefore, the equations (23), (24), and (25) in terms of $E_1, E_2, E_3, E_4, E_5, E_6$ are

$$\frac{\partial^2 V}{\partial x^2} + \frac{\partial^2 V}{\partial y^2} + \frac{Ha^2}{R_m} \frac{E_4}{E_1 E_3 E_4} \frac{\partial B}{\partial y} + \frac{Gr}{Re} T + 1 = 0, \tag{26}$$

$$\frac{\partial^2 B}{\partial x^2} + \frac{\partial^2 B}{\partial y^2} + R_m E_3 E_4 \frac{\partial V}{\partial y} = 0, \tag{27}$$

$$\frac{\partial^2 T}{\partial x^2} + \frac{\partial^2 T}{\partial y^2} + \frac{E_1}{E_6} P_r \left[\left(\frac{\partial V}{\partial x} \right)^2 + \left(\frac{\partial V}{\partial y} \right)^2 \right] + \frac{Ha^2 P_r}{R_m^2} \frac{E_4}{E_3^2 E_4^2 E_6} \left[\left(\frac{\partial B}{\partial x} \right)^2 + \left(\frac{\partial B}{\partial y} \right)^2 \right] = 0, \tag{28}$$

where

$Ha = B_0 a \sqrt{\frac{\sigma_f}{\mu_f}}$, is the Hartmann number,

$G_r = \frac{g\beta_f(T-T_0)a^3}{\nu_f^2}$, is the thermal Grashof number,

$P_r = \frac{\mu_f C_p}{k_f}$, is the Prandtl number,

$R_e = \frac{V_0 a}{\nu_f}$, is the Reynolds number,

and

$R_m = V_0 a(\mu_e)_f \sigma_f$, is the magnetic Reynolds number.

The corresponding boundary conditions (21) gives

$$\begin{aligned} V = 0, \quad B = 0, \quad T = 0, \quad \text{when } y = 0, \\ V = 0, \quad B = 0, \quad T = 0, \quad \text{when } y = 1, \\ V = 0, \quad B = 0, \quad T = 0, \quad \text{when } x = 0, \\ V = 0, \quad B = 0, \quad T = 0, \quad \text{when } x = 1. \end{aligned} \tag{29}$$

4. NUMERICAL TECHNIQUE AND GRID INDEPENDENCE STUDY

The dimensionless governing equations (26), (27), and (28) along with the boundary conditions (29) were discretized using the finite difference technique. In this numerical procedure, the computational domain is divided into a uniform grid system. Both the second-derivative and the squared first-derivative terms are discretized using the central difference of second-order accuracy. The finite difference form of $\partial^2 V / \partial x^2$ and $\partial V / \partial x$, for example, were discretized as $\frac{\partial^2 V}{\partial x^2} = \frac{V_{i+1,j} - 2V_{i,j} + V_{i-1,j}}{\Delta x^2} + O(\Delta x^2)$ and $\frac{\partial V}{\partial x} = \frac{V_{i+1,j} - V_{i-1,j}}{2\Delta x} + O(\Delta x^2)$, respectively. Therefore, the resultant difference equations become

$$V_{i,j} = A_3(V_{i+1,j} + V_{i-1,j}) + A_4(V_{i,j+1} + V_{i,j-1}) + A_5(B_{i,j+1} - B_{i,j-1}) + A_6(T_{i,j}) + A_7 \tag{31}$$

$$\begin{aligned} T_{i,j} = A_3(T_{i+1,j} + T_{i-1,j}) + A_4(T_{i,j+1} + T_{i,j-1}) + A_{12}(V_{i+1,j} - V_{i-1,j})^2 + \\ A_{13}(V_{i,j+1} - V_{i,j-1})^2 + A_{14}(B_{i+1,j} - B_{i-1,j})^2 + A_{15}(B_{i,j+1} - B_{i,j-1})^2. \end{aligned} \tag{32}$$

$$\begin{aligned} A_1 = \frac{Ha^2}{R_m} \frac{E_4}{E_1 E_3 E_4}, \quad A_2 = \frac{G_r}{R_e}, \quad A_3 = \frac{k^2}{2(h^2 + k^2)}, \quad A_4 = \frac{h^2}{2(h^2 + k^2)}, \quad A_5 = \frac{A_1 h^2 k}{2(h^2 + k^2)}, \quad A_6 = \frac{A_2 h^2 k^2}{(h^2 + k^2)}, \\ A_7 = \frac{h^2 k^2}{h^2 + k^2}, \quad A_8 = R_m E_3 E, \quad A_9 = \frac{A_8 h^2 k}{2(h^2 + k^2)}, \quad A_{10} = \frac{E_1}{E_6} P_r, \quad A_{11} = \frac{Ha^2 P_r}{R_m^2} \frac{E_4}{E_3^2 E_4^2 E_6}, \quad A_{12} = \frac{A_{10} k^2}{4(h^2 + k^2)}, \\ A_{13} = \frac{A_{10} h^2}{4(h^2 + k^2)}, \quad A_{14} = \frac{A_{11} k^2}{4(h^2 + k^2)}, \quad A_{15} = \frac{A_{11} h^2}{4(h^2 + k^2)} \end{aligned}$$

are constants, $\Delta x = h$ and $\Delta y = k$.

The corresponding discretized boundary conditions are:

$$\begin{aligned} V_{i,1} = 0, \quad B_{i,1} = 0, \quad T_{i,1} = 0, \quad \text{when } j = 1, \\ V_{i,m+1} = 0, \quad B_{i,m+1} = 0, \quad T_{i,m+1} = 0, \quad \text{when } j = n + 1, \quad \text{for } 1 \leq i \leq m + 1, \\ V_{1,j} = 0, \quad B_{1,j} = 0, \quad T_{1,j} = 0, \quad \text{when } i = 1, \\ V_{m+1,j} = 0, \quad B_{1,m+1} = 0, \quad T_{1,m+1} = 0, \quad \text{when } i = m + 1, \quad \text{for } 1 \leq j \leq n + 1. \end{aligned} \tag{33}$$

Using boundary conditions (32) the values $V_{i,j}$, $B_{i,j}$ and $T_{i,j}$ in the equations (30), (31), and (32) with the parameters (Ha) , (R_m) , (P_r) , (R_e) , (G_r) have been iterated. We have repeated the process, till the converged solution for $V_{i,j}$, $B_{i,j}$ and $T_{i,j}$ in the grid system are obtained.

5. RESULTS AND DISCUSSION

To obtain some physical insight into the problem, a numerical simulation has been constructed to justify the effect of various physical parameters that governed are by the system with the inclusion of various physical situations, on the

fluid variables, such as velocity, temperature, and induced magnetic field. The effect Hartmann number (Ha), Thermal Grashof number (Gr), Reynolds number (Re), Prandtl number (Pr) and magnetic Reynolds number (R_m) on the velocity, temperature, and induced magnetic field profiles are shown graphically.

The velocity profile of $Al_2O_3/Water$ nanofluid for different values of Hartmann number (Ha) is shown in Figure 2. It is observed that a rise in the Hartmann number causes a decrease in the velocity profile. This is due to the fact that when a magnetic field is applied to an electrically conducting fluid a Lorentz force is produced. This force retards the fluid velocity in the boundary layer region as the magnetic field opposes the transport phenomena.

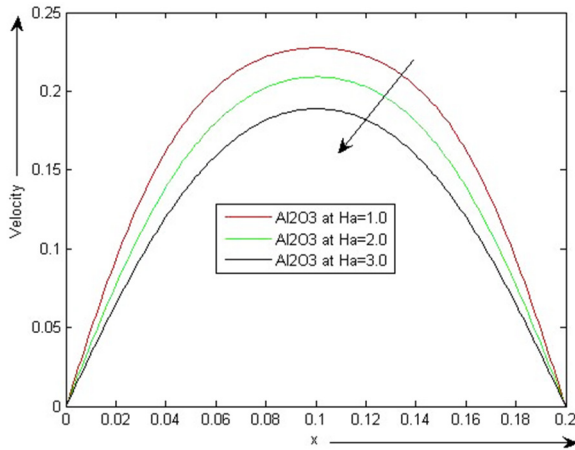


Figure 2. Effect of Hartmann number (Ha) on the velocity profile, when $Ha = 2, Pr = 0.71, R_m = 10, Gr = 2, Re = 10, h = k = 0.001, m = n = 200, \phi = 0.02, k_f = 40, k_s = 0.613$

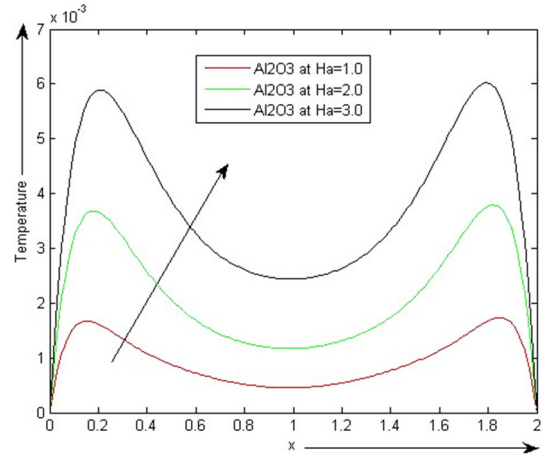


Figure 3. Effect of Hartmann number (Ha) on the temperature profile, when $Ha = 2, Pr = 0.71, R_m = 10, Gr = 2, Re = 10, h = k = 0.01, m = n = 200, \phi = 0.02, k_f = 40, k_s = 0.613$

On the other hand, in Figure 3, it is observed that the temperature distribution in the boundary layer region increases with the increase in Hartmann number (Ha). According to the Lorentz force effect, the flow encounters frictional resistance, which causes the boundary layer to heat up. In consequence, the temperature profile increases as (Ha) increase. The effect of magnetic fields on nanofluid has many industrial applications in the cooling sector also.

The effect of thermal Grashof number (Gr) on the velocity profile of $Al_2O_3/Water$ nanofluid is shown in Figure (4). Thermal Grashof number can be defined as the ratio of thermal buoyancy force to the viscous force in the boundary layer regime. With large values of this parameter, buoyancy dominates, and for small values viscosity dominates. In the above figure the velocity of $Al_2O_3/Water$ nanofluid is found to increase with the increase in thermal Grashof number (Gr). This means that the buoyancy force accelerates the velocity field. An increase in the value of the thermal Grashof number tends to induce much flow in the boundary layer due to the effect of thermal buoyancy. Again, it is found in Figure 5 that, the temperature of $Al_2O_3/Water$ nanofluid decreases with the increase in thermal Grashof number (Gr). This means that buoyancy force reduces the temperature field.

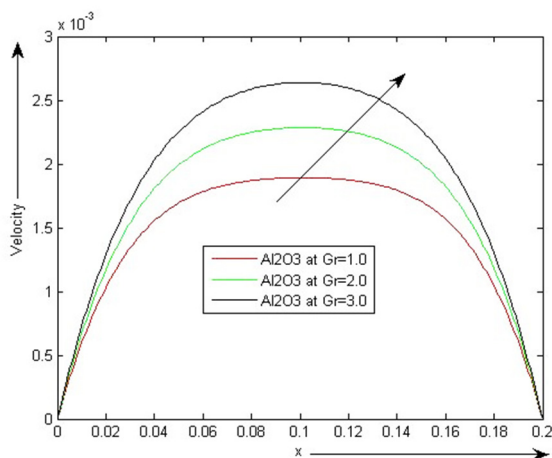


Figure 4. Effect Thermal Grashof number (Gr) on the velocity profile, when $Ha = 2, Pr = 0.71, R_m = 1, Gr = 6, Re = 1.5, h = k = 0.01, m = n = 200, \phi = 0.02, k_f = 40, k_s = 0.613$

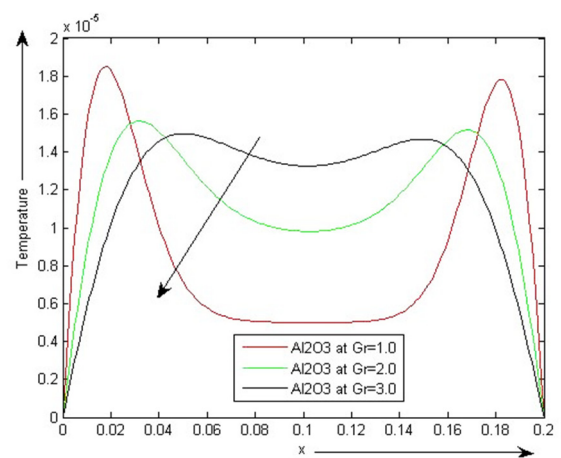


Figure 5. Effect Thermal Grashof number (Gr) on the temperature profile, when $Ha = 100, Pr = 1.0, R_m = 10, Gr = 2, Re = 1.5, h = k = 0.001, m = n = 200, \phi = 0.02, k_f = 40, k_s = 0.613$

Figure 6 shows the variation of the velocity field of $\text{Al}_2\text{O}_3/\text{Water}$ nanofluid for various values of Reynolds number (R_e). It is defined as the ratio of inertia force to viscous force. The Reynolds number depends on the relative internal movement due to different fluid velocities. For fluid flow analysis, the Reynolds number is considered to be a prerequisite. When viscous force dominates over the inertia force, the flow is smooth and at low velocities, the Reynolds number value is comparatively less, therefore velocity with $\text{Al}_2\text{O}_3/\text{Water}$ nanofluid decreases as Reynolds number increases. Again Figure 7 shows the variation of the temperature field of $\text{Al}_2\text{O}_3/\text{Water}$ nanofluid for various values of Reynolds number (R_e). It is seen that the temperature field increases as the (R_e) increases, and thus the rate of heat transfer is enhanced. However, the Reynolds number starts to decrease with temperature when the temperature exceeds the critical value depending on the corresponding concentration.

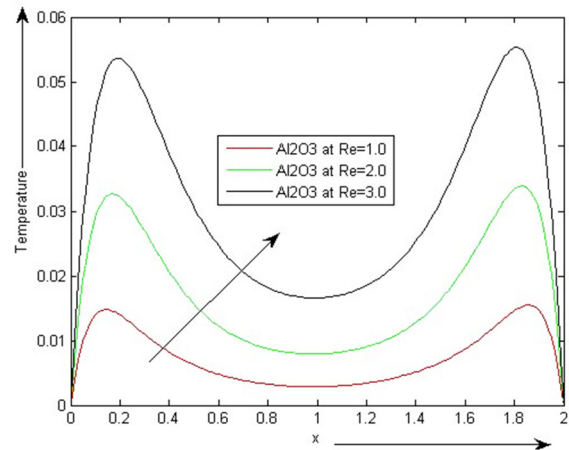
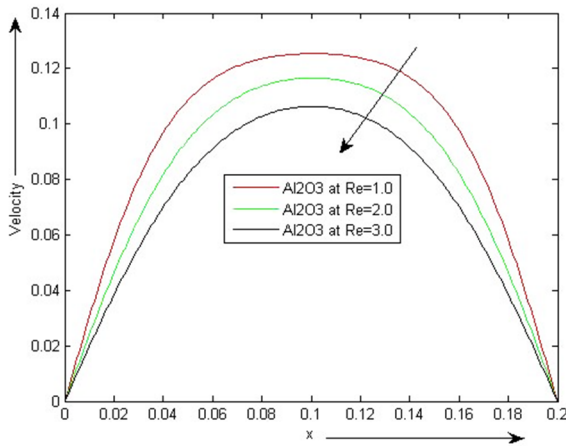


Figure 6. Effect Reynolds number (R_e) on the velocity profile, when $Ha = 5, P_r = 0.71, R_m = 5, G_r = 2, R_e = 10, h = k = 0.001, m = n = 200, \phi = 0.02, k_f = 40, k_s = 0.613$

Figure 7. Effect Reynolds number (R_e) on the temperature profile, when $Ha = 2, P_r = 6.93, R_m = 10, G_r = 2, R_e = 10, h = k = 0.01, m = n = 200, \phi = 0.02, k_f = 40, k_s = 0.613$.

The effect of Prandtl number (P_r) on velocity and temperature profiles is demonstrated graphically in Figures 8 and 9, respectively. It can be observed that the velocity of the nanofluid flow inside the boundary layer region increases whereas the temperature profile decreases due to an increase in Prandtl number (P_r). Prandtl number is the ratio of momentum diffusivity to thermal diffusivity. With a higher value of the Prandtl number, the momentum diffuses more rapidly than the heat, indicating that fluids with a higher Prandtl number have low thermal conductivity and a thinner thermal layer structure. This results in the temperature in the boundary layer region to decrease with the increase in the Prandtl number owing to the increase in the heat transfer rate of the fluid.

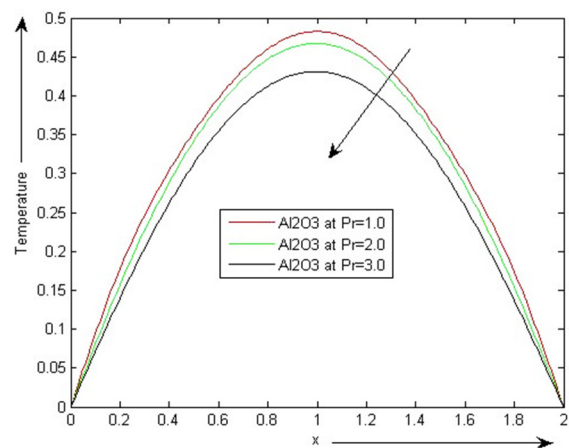
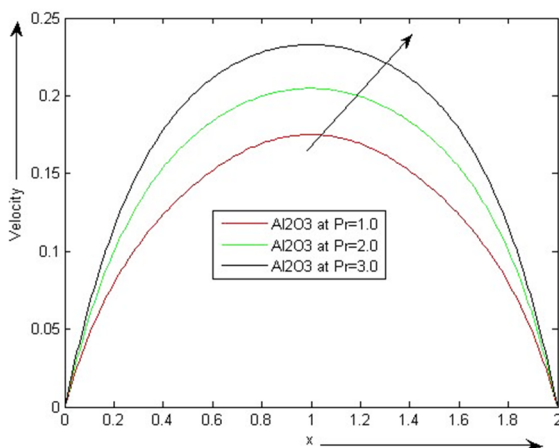


Figure 8. Effect Prandtl number (P_r) on the velocity profile, when $Ha = 2, P_r = 6.93, R_m = 5, G_r = 2, R_e = 1, h = k = 0.01, m = n = 200, \phi = 0.02, k_f = 40, k_s = 0.613$

Figure 9. Effect Prandtl number (P_r) on the temperature profile, when $Ha = 100, P_r = 0.71, R_m = 10, G_r = 2, R_e = 1, h = k = 0.01, m = n = 200, \phi = 0.02, k_f = 40, k_s = 0.613$

Figure 10 shows the variation of the velocity field of $\text{Al}_2\text{O}_3/\text{Water}$ nanofluid at various values of magnetic Reynolds number (R_m). It can be seen that the velocity profile rises with the increase in magnetic Reynolds number.

Again, Figure 11 shows the variation in the temperature profile of $\text{Al}_2\text{O}_3/\text{Water}$ nanofluid at various values of Magnetic Reynolds number (R_m). The magnetic Reynolds number is the magnetic analog of the Reynolds number, which is a fundamental dimensionless group that occurs in magnetohydrodynamics (MHD). It gives an estimate of the relative

effects of the advection or induction of a magnetic field by the motion of a conducting medium, often a fluid, to magnetic diffusion. Therefore, the temperature profile decreases as the value of (R_m) increases.

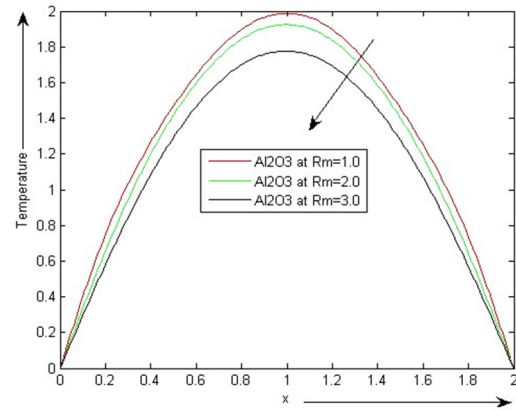
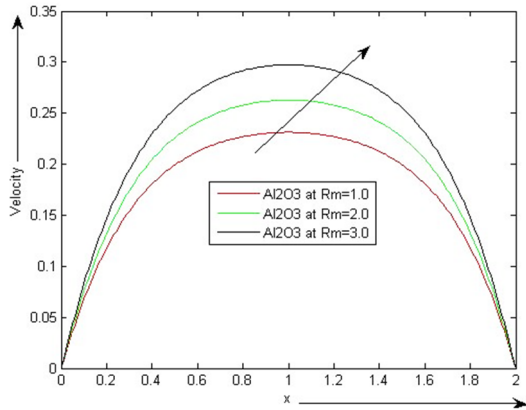
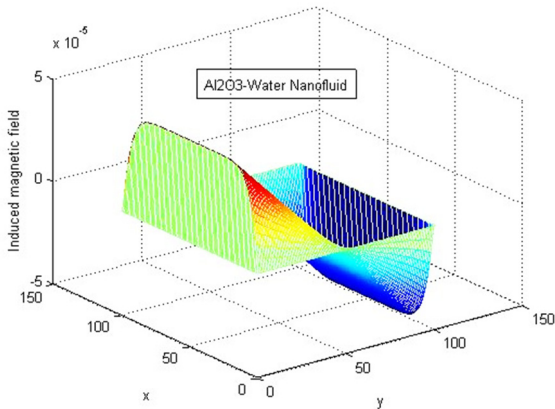


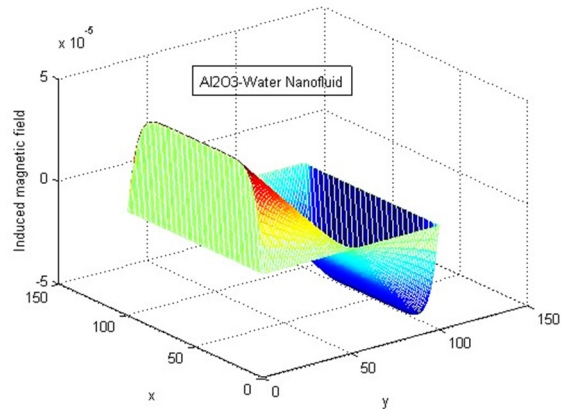
Figure 10. Effect Magnetic Reynolds number (R_m) on the velocity profile, when $Ha = 2, Pr = 6.93, R_m = 5, Gr = 2, Re = 1, h = k = 0.001, m = n = 200, \phi = 0.02, k_f = 40, k_s = 0.613$

Figure 11. Effect Magnetic Reynolds number (R_m) on the temperature profile, when $Ha = 100, Pr = 0.71, R_m = 1, Gr = 4, Re = 10, h = k = 0.01, m = n = 200, \phi = 0.02, k_f = 40, k_s = 0.613$

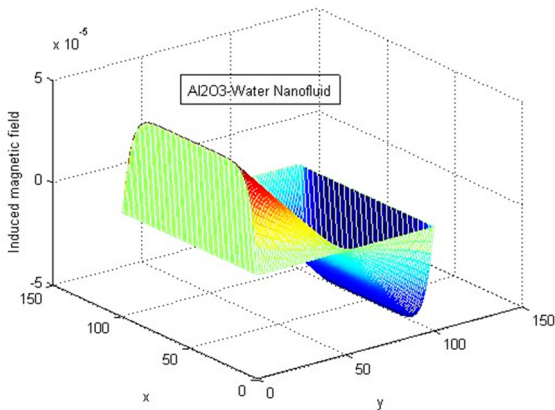
In Figures 12 (A), 12 (B), 12 (C), and 12 (D), the distribution of induced magnetic field B for mixed convection with the transverse magnetic field are plotted for $Ha = 100, Gr = 100; Ha = 200, Gr = 100, Ha = 300, Gr = 100; Ha = 400, Gr = 100$ and other parameters are fixed. It is observed that B becomes flattened for increasing values of Hartmann number Ha . Moreover, current lines and magnetic fields are almost orthogonal in almost all the duct cross-sections.



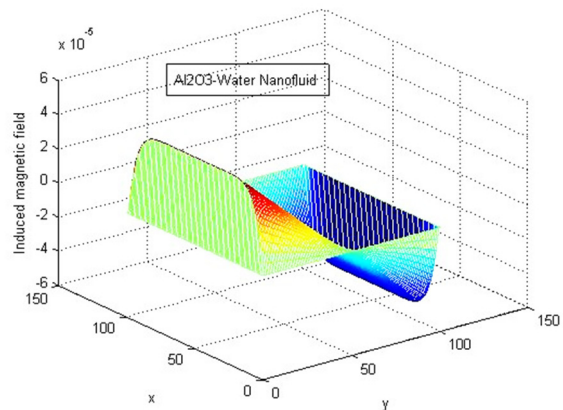
A



B



C



D

Figure 12. (A) Induced magnetic field for $Ha = 100$ and $Gr = 100$; (B) Induced magnetic field for $Ha = 100$ and $Gr = 200$; (C) Induced magnetic field for $Ha = 100$ and $Gr = 300$; (D) Induced magnetic field for $Ha = 100$ and $Gr = 400$

6. CONCLUSIONS

In the present exploration, we have made an investigation over the nanofluid flow (with base fluid water and nanoparticles as aluminum) through a square duct under the action of the strong transverse magnetic field. The numerical results are obtained by implementing the finite difference scheme coded in MATLAB software. The findings are summarized below:

- The velocity profile of the nanofluid declines with the increase in the value of the Hartmann number, whereas it increases with the increase in the value of the Prandtl number.
- The temperature profile of the nanofluid increase with the increase in Hartmann number and Reynolds number.
- The temperature profile of the nanofluid decelerates with the increase in the Prandtl number and Magnetic Reynolds number.
- The velocity profile of the nanofluid increase with the increase in the Prandtl number and Magnetic Reynolds number.
- The present study provides a model for enhanced heat transfer phenomena and hence finds its application in the cooling sector in industries, post-accidental heat removal in nuclear reactors, and heat exchangers. Besides these, some other important scientific applications of this study may be relevant to manufacturing industries, solar collectors, and so on.

Nomenclature

a	length of the cross-section of the square duct	p	Pressure force
\bar{B}	magnetic field	T	fluid temperature
B_0	applied magnetic field	T_0	wall temperature
C_p	specific heat at constant pressure	V	velocity in the z-direction
Ha	Hartmann number	x, y, z	Cartesian coordinates
G_r	Grashof number	β	coefficient of thermal expansion
R_e	Reynolds number	ρ_{nf}	density of nanofluid
P_r	Prandtl number	σ_{nf}	electrical conductivity of nanofluid
R_m	Magnetic Reynolds number	μ_{nf}	dynamic viscosity of nanofluid
g	acceleration due to gravity		

Subscripts

nf	nanofluids
f	Base Fluid
s	Solid particles of nanofluid

ORCID IDs

©Bishnu Ram Das, <https://orcid.org/0000-0002-9760-098X>; ©P.N. Deka, <https://orcid.org/0000-0001-9485-9294>
©Shiva Rao, <https://orcid.org/0000-0003-2055-4441>

REFERENCES

- [1] S.U.S. Choi, and J.A. Eastman, *Enhancing Thermal Conductivity of Fluids with Nanoparticles*, in *Developments and Applications of Non-Newtonian Flows*, edited by. D.A. Singer, and H.P. Wang, Vol. FED 231, (American Society of Mechanical Engineers, New York, 1995), pp. 99-105.
- [2] M.M. Doustdar, and M.K. Yekani, "Numerical study of mixed convection of nanofluid in a square duct containing hot obstacles," *Aerospace Mechanics Journal*, **12**, 67-78 (2016).
- [3] M.A. Mansour, R.A. Mohamed, M.M. Abd-Elaziz, and S.E. Ahmed, "Numerical simulation of mixed convection flows in a square duct partially heated from below using nanofluid," *International Communication Heat Mass Transfer*, **37**, 1504-1512 (2010), <https://doi.org/10.1016/j.icheatmasstransfer.2010.09.004>
- [4] B. Ghasemi, and S.M. Aminossadati, "Mixed convection in a square duct filled with nanofluids," *International Commun. Heat Mass Transfer*, **37**, 1142-1148 (2010), <https://doi.org/10.1016/j.icheatmasstransfer.2010.06.020>
- [5] E. Abu-Nada, and H.F. Oztop, "Effects of inclination angle on natural convection in enclosures filled with Cu/water nanofluid," *International Journal Heat Fluid Flow*, **30**, 669-678 (2009), <https://doi.org/10.1016/j.ijheatfluidflow.2009.02.001>
- [6] E.M. Hemmat, I. Akbari, and A. Karimipour, "Mixed convection in a square duct with an inside hot obstacle filled by an Al_2O_3 /water nanofluid," *Journal Applied Mechanics Technology Physics*, **56**, 443-453 (2015), <https://doi.org/10.1134/S0021894415030141>
- [7] M.K. Moallemi, and K.S. Jang, "Prandtl number effects on laminar mixed convection heat transfer in a lid-driven cavity," *International Journal of Heat Mass Transfer*, **35**, 1881-1892 (1992), [https://doi.org/10.1016/0017-9310\(92\)90191-T](https://doi.org/10.1016/0017-9310(92)90191-T)
- [8] O. Aydin, and W.J. Yang, "Mixed convection in cavities with a locally heated lower wall and moving sidewalls," *Numerical Heat Transfer: Part A: Applications*, **37**, 695-710 (2000), <https://doi.org/10.1080/104077800274037>
- [9] H.F. Oztop, and I. Dagitkin, "Mixed convection in square duct differentially heated square cavity," *International Journal of Heat and Mass Transfer*, **47**, 1761-1769 (2004), <https://doi.org/10.1016/j.ijheatmasstransfer.2003.10.016>
- [10] K.V. Wong, and O. De Leon, "Applications of Nanofluids: Current and Future," *Advances in Mechanical Engineering*, Article ID 519659, (2010), <https://doi.org/10.1155/2010/519659>
- [11] Y. Li, H.-Q. Xie, W. Yu, and J. Li, "Investigation on Heat Transfer Performances of Nanofluids in Solar Collector," *Materials Science Forum*, **694**, 33-36 (2011). <https://doi.org/10.4028/www.scientific.net/MSF.694.33>
- [12] T. Yousefi, F. Veysi, E. Shojaeizadeh, and S. Zinadini, "An experimental investigation on the effect of Al_2O_3 /Water nanofluid on the efficiency of solar flat plate collectors," *Renewable Energy*, **39**(1), 293-298 (2011), <https://doi.org/10.1016/j.renene.2011.08.056>

- [13] R.A. Taylor, P.E. Phelan, T. Otanicar, C.A. Walker, M. Nguyen, S. Trimble, and R. Prasher, "Applicability of Nanofluids in High Flux Solar Collectors," *Journal of Renewable and Sustainable Energy*, **3**(2), 023104 (2011), <http://dx.doi.org/10.1063/1.3571565>
- [14] B.C. Pak, and Y.I. Cho, "Hydrodynamic and heat transfer study of dispersed fluids with submicron metallic oxide particle," *Exp. Heat Transfer*, **11**, 151 (1998), <https://doi.org/10.1080/08916159808946559>
- [15] W. Yu, and S.U.S. Choi, "The role of interfacial layers in the enhanced thermal conductivity of nanofluids; a renovated Maxwell model," *Journal Nanoparticles Res.* **5**, 167-171 (2003), <https://doi.org/10.1023/A:1024438603801>
- [16] Y. Xuan, and W. Roetzel, "Conceptions for heat transfer correlation of nanofluids," *International Journal Heat Mass Transfer*, **43**, 3701-3707 (2000), [http://dx.doi.org/10.1016/S0017-9310\(99\)00369-5](http://dx.doi.org/10.1016/S0017-9310(99)00369-5)
- [17] J. Rahimah, R. Nazar, and I. Pop, "Magnetohydrodynamic boundary layer flow and heat transfer of nanofluids past a bidirectional exponential permeable stretching/shrinking sheet with viscous dissipation effect," *Journal Heat Transfer*, **141**, 012406 (2019), <https://doi.org/10.1115/1.4041800>
- [18] T.-C. Hung, and W.-M. Yan, "Enhancement of thermal performance in double-layered microchannel heat sink with nanofluids," *International Journal Heat Mass Transfer*, **55**, 3225-3238 (2012), <https://doi.org/10.1016/j.ijheatmasstransfer.2012.02.057>
- [19] M. Sheikhpour, M. Arabi, A. Kasaeian, A.R. Rabei, and Z. Taherian, "Role of nanofluids in drug delivery and biomedical technology: methods and applications," *Nanotechnol. Sci. Appl.* **13**, 47 (2020), <https://doi.org/10.2147%2FNSA.S260374>
- [20] S.D. Majumder, and A. Das, "A short review of organic nanofluids: preparation, surfactants, and applications," *Front. Mater.* **8**, 630182 (2021), <https://doi.org/10.3389/fmats.2021.630182>
- [21] M.S. Dehaj, M. Rezaeian, and D. Mousavi, S. Shamsi, and M. Salarmofrad, "Efficiency of the parabolic through solar collector using $NiFe_2O_4$ /water nanofluid and U-tube," *Journal Taiwan Inst. Chem. Eng.* **120**, 136-149 (2021), <https://doi.org/10.1016/j.jtice.2021.02.029>
- [22] R. Sivaraj, and S. Banerjee, "Transport properties of non-Newtonian nanofluids and applications," *The European Physical Journal Special Topics*, **230**, 1167-1171 (2021), <https://doi.org/10.1140/epjs/s11734-021-00031-1>
- [23] T. Thumma, A. Wakif, and I.L. Animasaun, "Generalized differential quadrature analysis of unsteady three-dimensional MHD radiating dissipative Casson fluid conveying tiny particles," *Heat Transfer*, **49**(5), 2595-2626 (2020), <https://doi.org/10.1002/htj.21736>
- [24] S. Lahmar, M. Kezzar, M.R. Eid, and M.R. Sari, "Heat transfer of squeezing unsteady nanofluid flow under the effects of an inclined magnetic field and variable thermal conductivity," *Physica A*, **540**, 123-138 (2020), <https://doi.org/10.1016/j.physa.2019.123138>
- [25] N.C. Roşca, and I. Pop, "Hybrid nanofluids flows determined by a permeable power-Law stretching/shrinking sheet modulated by orthogonal surface shear," *Entropy*, **23**(7), 813 (2021), <https://doi.org/10.3390/e23070813>
- [26] F. Selimefendigil, and H.F. Oztop, "Thermal management and modeling of forced convection and entropy generation in a vented cavity by simultaneous use of a curved porous layer and magnetic field," *Entropy*, **23**(2), 152 (2021), <https://doi.org/10.3390/e23020152>
- [27] W. Jamshed, "Numerical investigation of MHD impact on Maxwell nanofluid," *International Commun. Heat Mass Transfer*, **120**, 104973 (2021), <https://doi.org/10.1016/j.icheatmasstransfer.2020.104973>
- [28] W. Jamshed, K.S. Nisar, and R.W. Ibrahim, "Computational frame work of Cattaneo-Christov heat flux effects on Engine Oil based Williamson hybrid nanofluids: a thermal case study," *Case Stud. Therm. Eng.* **26**, 101179 (2021), <https://doi.org/10.1016/j.csite.2021.101179>
- [29] W. Jamshed, "Thermal augmentation in solar aircraft using tangent hyperbolic hybrid nanofluid: a solar energy application," *Energy Environ.* **33**(6), 1-44 (2021), <https://doi.org/10.1177/09583305X211036671>
- [30] S. Rao, and P. Deka, "A Numerical Study on Unsteady MHD Williamson Nanofluid Flow past a Permeable Moving Cylinder in the presence of Thermal Radiation and Chemical Reaction," *Biointerface Research in Applied Chemistry*, **13**(5), 1-19 (2023), <https://biointerfaceresearch.com/wp-content/uploads/2023/01/BRIAC135.436.pdf>
- [31] S. Rao, and P. Deka, "A Numerical Study on Heat Transfer for MHD Flow of Radiative Casson Nanofluid Over a Porous Stretching Sheet," *Latin American Applied Research – an International Journal*, **53**(2), 129-136 (2023), <https://doi.org/10.52292/j.laar.2023.950>
- [32] T.A. Yusuf, R.N. Kumar, R.J.P. Gowda, and U.D. Akpan, "Entropy generation on flow and heat transfer of a reactive MHD Sisko fluid through inclined walls with porous medium," *Int. J. Ambient Energy*, **43**(1), 6307-6316 (2022), <https://doi.org/10.1080/01430750.2021.2013941>
- [33] H.K. Hamzah, F.H. Ali, and M. Hatami, "MHD mixed convection and entropy generation of CNT-water nanofluid in a wavy lid-driven porous enclosure at different boundary conditions." *Sci. Rep.* **12**, 2881 (2022), <https://doi.org/10.1038/s41598-022-06957-3>
- [34] W.U. Khan, M. Awais, N. Parveen, A. Ali, S.E. Awan, M.Y. Malik, and Y. He, "Analytical Assessment of (Al_2O_3 -Ag/ H_2O) Hybrid Nanofluid Influenced by Induced Magnetic Field for Second Law Analysis with Mixed Convection," *Viscous Dissipation and Heat Generation, Coatings*, **11**, 498 (2021), <https://doi.org/10.1038/s41598-022-06957-3>
- [35] S. Ahmed, and I. Pop, "Mixed convection boundary layer flow from a vertical flat plate embedded in a porous medium filled with nano-fluids," *Int. Commun. Heat Mass Transf.* **37**, 987-999 (2010), <https://doi.org/10.1016/j.icheatmasstransfer.2010.06.004>
- [36] A. Malvandi, and D.D. Ganji, "Mixed convection of alumina-water nanofluid inside a concentric annulus considering nanoparticle migration," *Particology*, **24**, 113-122 (2016), <https://doi.org/10.18869/acadpub.jafm.68.236.25641>
- [37] T. Tayebi, and A.J. Chamkha, "Magnetohydrodynamic Natural Convection Heat Transfer of Hybrid Nanofluid in a Square Enclosure in the Presence of a Wavy Circular Conductive Cylinder," *Journal Therm. Sci. Eng. Appl.* **12**(3), 031009 (2020), <https://doi.org/10.1115/1.4044857>
- [38] Z. Shah, P. Kumam, and W. Deebani, "Radiative MHD Casson Nanofluid Flow with Activation energy and chemical reaction over past nonlinearly stretching surface through Entropy generation," *Sci.* **10**(1), 1-14 (2020), <https://doi.org/10.1038/s41598-020-61125-9>
- [39] V. Rajesh, M. Srilatha, and A.J. Chamkha, "Hydromagnetic effects on hybrid nanofluid Cu- Al_2O_3 /Water flow with convective heat transfer due to a stretching sheet," *Journal Nanofluids*, **9**(4), 293-301 (2020), <https://doi.org/10.1166/jon.2020.1755>
- [40] S. Molli, and K. Naikoti, "MHD Natural Convective Flow of Cu-Water Nanofluid over a Past Infinite Vertical Plate with the Presence of Time Dependent Boundary Condition," *International Journal Thermofluid Sci. Technol.* **7**(4), 1-15 (2020), <https://doi.org/10.36963/IJTST.2020070404>

- [41] N.S. Khashi'ie, N.M. Arifin, I. Pop, and N.S. Wahid, "Flow and heat transfer of hybrid nanofluid over a permeable shrinking cylinder with Joule heating: A comparative analysis," *Alexandria Eng. Journal*, **59**(3), 1787-1798 (2020), <https://doi.org/10.1016/j.aej.2020.04.048>
- [42] W. Alghamdi, T. Gul, M. Nullah, A. Rehman, S. Nasir, A. Saeed, and E. Bonyah, "Boundary layer stagnation point flow of the Casson hybrid nanofluid over an unsteady stretching surface," *AIP Adv.* **11**(1), 015016 (2021), <https://doi.org/10.1063/5.0036232>
- [43] M. Shahzad, M. Ali, F. Sultan, W.A. Khan, and Z. Hussain, "Computational investigation of magneto-cross fluid flow with multiple slip along wedge and chemically reactive species", *Results Phys.* **16**, 102972 (2020), <https://doi.org/10.1016/j.rinp>
- [44] N. Ibrar, M.G. Reddy, S.A. Shehzad, P. Sreenivasulu, and T. Poornima, "Interaction of single and multi-walls carbon nanotubes in magnetized-nano casson fluid over radiated horizontal needle," *SN Appl. Sci.* **2**, 677 (2020), <https://doi.org/10.1007/s42452-020-2523-8>
- [45] L.A. Lund, Z. Omar, J. Raja, I. Khan, and E.M. Sherif, "Effects of Stefan blowing and slip conditions on unsteady MHD casson nanofluid flow over an unsteady shrinking sheet: dual solutions," *Symmetry*, **12**, 487 (2020), <https://doi.org/10.3390/sym12030487>
- [46] S. Rao, and P. Deka, A Numerical investigation on Transport Phenomena in a Nanofluid Under the Transverse Magnetic Field Over a Stretching Plate Associated with Solar Radiation. *Nonlinear Dynamics and Applications*, **2022**, 473-492, https://doi.org/10.1007/978-3-030-99792-2_39
- [47] S. Rao, and P. Deka, "A numerical solution using EFDM for unsteady MHD radiative Casson nanofluid flow over a porous stretching sheet with stability analysis," *Heat Transfer*, **51**(8), 8020-8042 (2022), <https://doi.org/10.1002/htj.22679>
- [48] H.C. Brinkman, "The viscosity of concentrated suspensions and solutions," *J. Chem. Phys.* **20**, 571-581 (1952), <https://doi.org/10.1063/1.1700493>
- [49] W.A. Khan, M. Ali, F. Sultan, M. Shahzad, M. Khan, and M. Irfan, "Numerical interpretation of autocatalysis chemical reaction for nonlinear radiative 3D flow of Cross magnetofluid," *Pramana J. Phys.* **92**, 16 (2019), <https://doi.org/10.1007/s12043-018-1678-y>
- [50] J.A. Maxwell, *Treatise on Electricity and Magnetism*, second ed. (Oxford University Press, Cambridge, 2010).
- [51] K. Khanafer, K. Vafai, and M. Lightstone, "Buoyancy-driven heat transfer enhancement in a two-dimensional enclosure utilizing nanofluids," *Int. J. Heat Mass. Transf.* **46**, 3639-3653 (2003), [https://doi.org/10.1016/S0017-9310\(03\)00156-X](https://doi.org/10.1016/S0017-9310(03)00156-X)

ЧИСЛОВИЙ АНАЛІЗ МГД ЗМІШАНОГО КОНВЕКЦІЙНОГО ПОТОКУ НАНОРІДИНИ Al_2O_3/H_2O (АЛЮМІНІЙ-ВОДА) У ВЕРТИКАЛЬНОМУ КВАДРАТНОМУ КАНАЛІ

Бішну Рам Дас, П.Н. Дека, Шива Рао

Факультет математики, Університет Дібругарх, Дібругарх-786004, Ассам, Індія

У цій роботі ми розглянули стаціонарну ламінарну магнітогідродинамічну (МГД) змішану конвекцію електропровідної рідини в присутності наночастинок Al_2O_3 , тоді як вода є основною рідиною у вертикальному квадратному каналі. Стінки воздуховода утеплені. У рівнянні енергії також враховується ефект в'язкої дисипації та джоулева теплота. У цьому випадку на стінках каналу підтримується постійна температура. Використовуючи безрозмірні величини, керівні рівняння імпульсу, індукції та енергії спочатку перетворюються на безрозмірні рівняння, а потім скорочені рівняння розв'язуються за допомогою явного методу кінцевих різниць. Профілі швидкості, температури та індукованого магнітного поля будуються графічно для аналізу впливу різних параметрів потоку. Помічено, що рух нанофлюїду прискорюється зі збільшенням значення магнітного параметра, числа Рейнольдса та числа Прандтля. Сучасні дослідження можуть знайти застосування в багатьох галузях промисловості та охолодження. У цьому дослідженні відзначено його важливість для підвищення ефективності теплопередачі для практичних застосувань, пов'язаних із промисловістю та технікою. Проблеми, які обговорюються в цьому дослідженні, не були включені в попередні дослідження сталого потоку нанофлюїдів через квадратну трубу.

Ключові слова: нанофлюїди; явний чисельний метод кінцевих різниць (EFDM); МГД потік; сила виштовхування; змішана конвекція; квадратний повітропровід; теплопередача; магнітне поле